Results in Materials 11 (2021) 100218

Contents lists available at ScienceDirect

Results in Materials

journal homepage: www.sciencedirect.com/journal/results-in-materials

Optimising compression testing for strain uniformity to facilitate microstructural assessment during recrystallisation

Carl Slater *, Nusrat Tamanna, Claire Davis

WMG, University of Warwick, Coventry, CV4 7AL, UK

ARTICLE INFO

Keywords:
Strain homogeneity
Thermo-mechanical testing
Recrystallisation

ABSTRACT

Predicting the kinetics of recrystallisation in metals, and recrystallised grain size distributions, is one the key approaches to controlling and refining grain size during metal processing, which typically increases strength and toughness/ductility. Recrystallisation prediction models and equations are supported by lab-based simulations that can systematically assess recrystallisation over a range of temperatures and strains for different materials and starting grain sizes. This work uses modelling and experimental verification to assess the different commonly used compression test sample geometries to determine strain uniformity and potential sources of error in microstructural assessment and proposes a modified geometry that increases the area of constant known strain. Whilst flow stress measurements in all samples showed good agreement. It has been shown that the new plane strain geometry offers a more consistent, homogeneous strain through the sample such that the large number of grains needed for accurate grain size distribution measurement can be readily achieved. Over double the area of ±10% of the target strain was achieved in the modified plane strain sample compared to a conventional uniaxial specimen, this area was also shown to be more conducive to metallographic assessment and offers in excess of 1500 grains of 250 μm to be assess per cross-sectional slice.

1. Introduction

Recrystallisation can be one of the most effective ways of refining grain sizes in metallic structures. In many manufacturing processes parts are not produced to final geometry through casting and need subsequent processing, such as hot rolling or forging, to achieve the desired shape. The additional processing can give added benefit of grain refinement via recrystallisation using the deformation stored energy. This mechanism is heavily used across many industries such as steel [1], nickel super alloys [2], copper [3] and aluminium [4] and is most prevalent in production methods such as hot rolling, forging [1] and cold rolled/annealed processing [5]. Whilst many materials can show significant refinement through other means during casting and heat treatments [6,7] through nucleation control, recrystallisation remains a dominant field of interest across metallic material.

Recrystallisation is an essential tool for steel processing to achieve properties and development of fundamental understanding and predictive models has been harnessed to drive product developments. Since its first implementation in the 1950's thermo-mechanically controlled rolling (TMCR) has proven to be invaluable in the steel industry. By controlling reheating and the amount of rolling reduction around critical temperatures, such as the microalloy precipitate dissolution temperature and the TNR (temperature of no recrystallisation), then strength can be seen to increase >20% in conventional C–Mn steel [8] and TMCR has been instrumental in the development of high strength low alloy (HSLA) and advanced high strength steels (AHSS), which show superior strength/elongation ratios [9].

No single experimental method is used to determine recrystallisation behaviour, or to provide data to support/validate recrystallisation models, encompassing the full range of temperatures, strains and strain rates experienced for different materials and processing conditions. Uniaxial compression tests (UCT), plane strain compression tests (PSCT) and torsion tests (TT) are used to study the hot deformation behaviour (flow stresses) and evolution of microstructure for metals (particularly steel), for example supporting the development of predictive equations for recrystallisation [10–12] during hot rolling/forging. A lot of recrystallisation studies have used load feedback during the tests, either through double hit testing [13] or stress relaxation testing [14], to obtained a rapid assessment of the flow stresses and rates of recrystallisation, which also allow predictions of the mill loads needed to roll at a

* Corresponding author.
E-mail address: c.d.slater@warwick.ac.uk (C. Slater).

https://doi.org/10.1016/j.rinma.2021.100218
Received 14 July 2021; Received in revised form 2 August 2021; Accepted 13 August 2021
Available online 18 August 2021

specific temperature. Flow stress measurements at a given temperature are affected by recovery, recrystallisation and grain size which means it is difficult to identify the exact contribution of each or to determine microstructural parameters such as recrystallised grain size distributions from these types of tests.

Assessment of recrystallisation fraction and recrystallised grain sizes can be carried out using UCT, PSCT and TT with interrupted quenching of the sample to observe the microstructure for different strain, strain rate, temperature and hold times. UCT and PSCT are the most common approaches for microstructural evaluation with systems such as Gleeble [15] or Servotest [16] allowing rapid assessment. However, a drawback of these methods is the barrelling effect due to friction at the interface between the sample and anvils [17]. This leads to a characteristic strain distribution with "dead zones" at either end of the sample, by the anvils, and a high strain concentration in the sample centre. The inhomogeneity in strain distribution was reported by Chamanfar et al. [18] for uniaxial deformation of 10 mm Ø x 15 mm cylindrical samples deformed with 0.83 macroscopic strain and a 0.1 friction coefficient. The predicted strain in the dead zone was 0.6 and the peak strain reached 1.1 in the centre of the sample. Bennett et al. [19] developed FEM models of both isothermal axisymmetric compression and uniaxial compression testing and compared the predictions to measured flow stress behaviour using the Gleeble thermo-mechanical simulator. It was found that the errors in stress prediction and measurement can be as large as 20% due to the non-uniform deformation caused by interfacial friction between the sample and anvils, generated heat during deformation and a non-uniform temperature field. Strain inhomogeneity means that microstructural examination needs to be undertaken with care in order for the measured grain size to be related to the imposed local strain.

Torsion allows much higher strains and strain rates to be imposed than for UCT and PSCT, for example enabling large strain multi-pass rolling/forging schedules to be simulated in one test [12,20]. A disadvantage of this method is the presence of a strong strain gradient through the radial axis of the sample, resulting in very limited material with uniform strain for microstructural analysis (with added complication in relating the microstructure to imposed local strain at the location characterised) and stress measurements being averaged across the whole sample. In order to precisely understand the local strain regions in torsion testing, then this is commonly coupled with finite element modelling with dynamic recrystallisation, work hardening etc impacting the location used for optical analysis [21]. This testing has been successfully carried out at some institutes for which it has been used for multipass rolling simulations [12], however accuracy of this method relies on modelling and careful experimentation by experienced users due to the large strain fields produced. Forrest and Sinfield [22] showed that for a single 360° rotation then the volumetric strain varies across the radial plane at the central length position between 0.8 and 2 for a standard 9.5 mm diameter hollow sample with a 2.4 mm wall thickness, resulting in a range of strain rates from 3 to 34 s^{-1}. Under these conditions there will be a strain gradient across individual grains (assuming a prior austenite grain size of 250 μm, representative of a typical reheated steel slab grain size, with a strain variation of 0.1 occurring over that length scale) indicating the challenge when trying to assess grain size changes due to recrystallisation.

To compensate for the strain inhomogeneity that arises fitting parameters/corrections have been proposed to relate the measured flow stress from the UCT, PSCT or TT to the macroscopic measured flow behaviour of the material [17,23,24]. However, for microstructural characterisation to relate microstructural parameters to applied strain/strain rate there is a need for samples that provide sufficiently large areas of homogeneous strain for hundreds of grains to be characterised. This is particularly important for measurements such as full recrystallised grain size distributions [25] and the influence of segregation on recrystallisation kinetics [26]. This paper reports on the strain inhomogeneity in standard UCT and PSCT samples used in thermo-mechanical simulations, modelled using FEM and verified experimentally and proposes alternate sample configurations to provide larger areas of uniform strain for microstructural characterisation.

2. Methodology

2.1. Finite element modelling

The three most common sample geometries used for UCT and PSCT, summarised in Table 1, were modelled initially to determine the strain distribution across the samples. Modified sample geometries were also determined to provide increased strain uniformity and area of known strain, discussed in the results section.

Deform v12.0.1 software was used to model the strain distribution for the three geometries in Table 1. A macroscopic strain of 0.3 was applied at a strain rate of 1 s^{-1}. The anvils were considered rigid bodies of 10 mm thickness with a 7° draft angle. The test simulations were carried out at room temperature so any influence of thermal conductivity can be neglected in this investigation. A friction coefficient of 0.15 was used as contact conditions between the sample and the anvils in all conditions, this was verified through measurement of the barrelling observed after deformation and is consistent with literature [18,19,30].

Histograms for the area corresponding to different strain values were generated from the simulations by remeshing the surface of the y-z plane at x = 0 (centre of deformation) ensuring a consistent mesh volume.

3. Materials and experimental details

Verification of the modelling was carried out using stainless steel 316 that was initially annealed at 1050 °C for 1hr to ensure a fully recrystallised microstructure [31].

Compression testing was carried out in a Gleeble HDS-V40, three tested were carried out in each condition. Uniaxial compression testing was carried out using 0.1 mm graphite foil and 0.1 mm tantalum foil on both contact surfaces (to be consistent with high temperature testing [23,27]). Deformation was carried out at a strain rate of 1 s^{-1} to a strain of 0.3.

All samples were sectioned using a 1 mm diamond blade on a Buehler Isomet precision cutter before mounting in Bakelite and polishing to a ¼ micron finish. Microhardness was carried out using a Wilson VH3300 microhardness system with a load of 500 g. Indents were spaced at 250 μm intervals and 500 μm away from the outside edge of the sample. Hardness values were converted to stress using $\Delta\sigma_y = 3.03\Delta H$, where $\Delta\sigma_y$ is the change in stress (MPa) and ΔH is the change in hardness. This equation was taken from the literature and shows a regression fit of 0.88 for a ΔH of up to 300Hv for a range of austenitic stainless steels [32]. To determine the strain distribution in the deformed sample the measured hardness values were converted to strength values and the strength was the correlated to the imposed strain required to generate that strength, using Fig. 1. Fig. 1 was generated using a UCT1 sample on a HDS V40 Gleeble to a strain of 0.55.

Table 1
Summary of compression test simulations.

Sample	Sample Geometry commonly used	Anvil Geometry	Reference
UCT1	Cylinder 10 mm Ø x 15 mm length[a]	20 mm Ø	[27]
UCT2	Cylinder 10 mm Ø x 12 mm length	20 mm Ø	[23]
PSCT	10 × 15 × 20mm (HxWxL)[b]	10 × 80 mm	[28,29]

[a] Exact dimensions vary in the literature, however 1.5–2 aspect ratio (length: diameter) is typically used and has been considered in this work.

[b] 10 × 15 × 50mm was used in this study. The length of the sample does not influence the straining of the material (verified by modelling) and a longer sample was used to accommodate the experimental verification setup on the Gleeble HDS-V40.

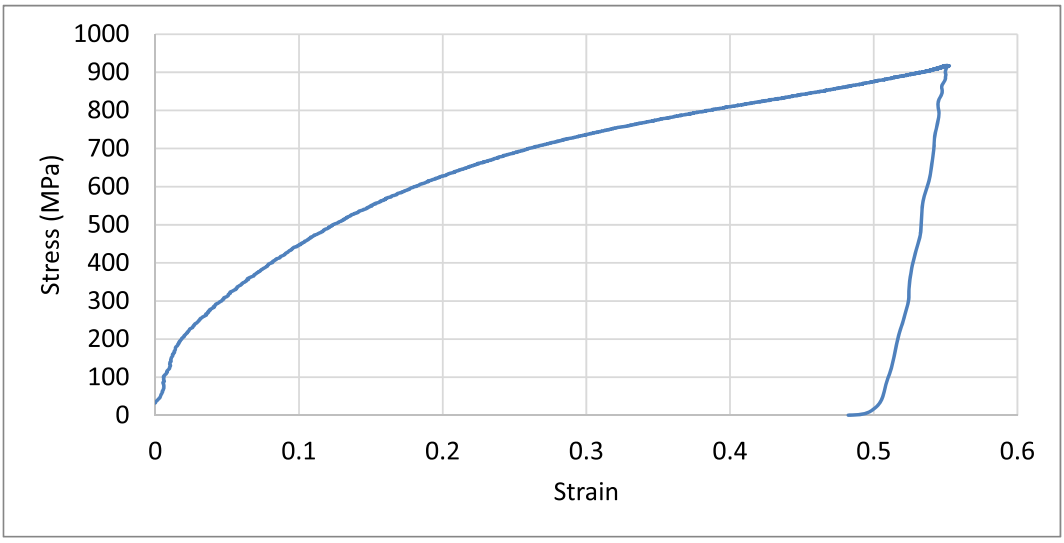

Fig. 1. Stress-strain plot for the stainless steel 316 used in this study.

4. Results and discussion

4.1. Uniaxial compression

The predicted strain distribution in sample UCT1 is given in Fig. 2 after deformation to a macroscopic imposed strain of 0.3. It can be seen clearly that a strong strain distribution exists throughout the sample. Due to the interfacial friction between the sample and anvils, barrelling occurs which leads to a very typical "cross" shape strain map with high strains in the sample corners. Whilst the mean strain across the sample is 0.278, close to the imposed macroscopic strain, the strain at the core shows a much higher value of 0.44. Any microstructural evaluation, for example to relate recrystallised grain size to strain, is challenging due to the strain variation – for example the need to know the exact location of the microstructural measurement to relate to the local strain and limited area of uniform strain.

Fig. 3a shows the spatial distribution of the strain that falls within ±10% of the 0.3 applied macroscopic strain. The total area shown equates to around 34.8% of the sample, or 52 mm^2, for the sample cross section. This microstructural area will equate to that occupied by around 700 grains with an equivalent circle diameter of 250 μm (i.e. typical of a reheated prior austenite grain size for steels prior to TMCR), this is at the minimum that has been suggested to be measured to obtain a full grain size distribution for recrystallisation kinetics (where 700–1000 [33] or even 2000 grains [34] have been reported), but would be sufficient to assess mode grain size. Not only is this a reasonably small region, but the distribution of this field would make consistent sectioning and metallurgical assessment difficult (further discussion on sectioning sensitivity is discussed later). There is, however, a region of reasonably uniform, albeit higher strain, in the centre of the sample, Fig. 3b. This region can be seen to have a strain of 0.38–0.44 (average of 0.4) and only comprises 9% of the cross sectional area of the sample, which would allow a maximum of 180 grains of 250 μm to be measured from a single section.

This sample geometry gives high strain at the corners and a dead zone at either end of the sample. At high temperatures this can be further exacerbated by the presence of a thermal profile along the length of the sample (from the cooler anvils), giving rise to increased strain inhomogeneity.

It is important to consider the friction effects and thermal gradients affect barrelling, and hence strain inhomogeneity, which can be determined using the following equation:

$$B = \frac{h_f D_f^{\,2}}{h_o D_o^{\,2}} \tag{1}$$

Where B is the barrelling coefficient, h_o and h_f are the initial and final height of the specimen. D_o and D_f are the initial and final diameter at the

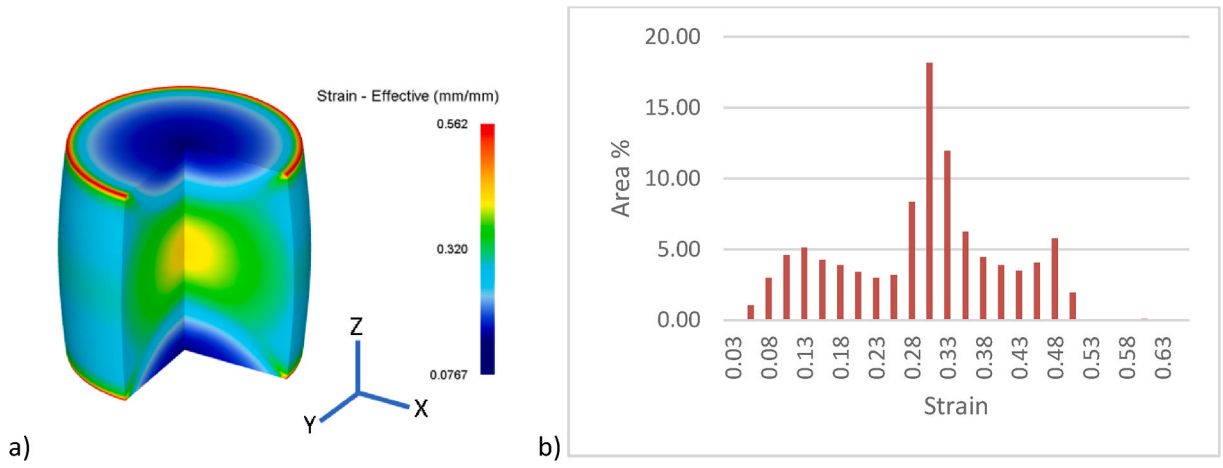

Fig. 2. a) Strain distribution in Uniaxial 1 sample at a macroscopic strain of 0.3 b) histogram showing the sample area fraction experiencing the different strain levels in the Y-Z plane (as X = 0).

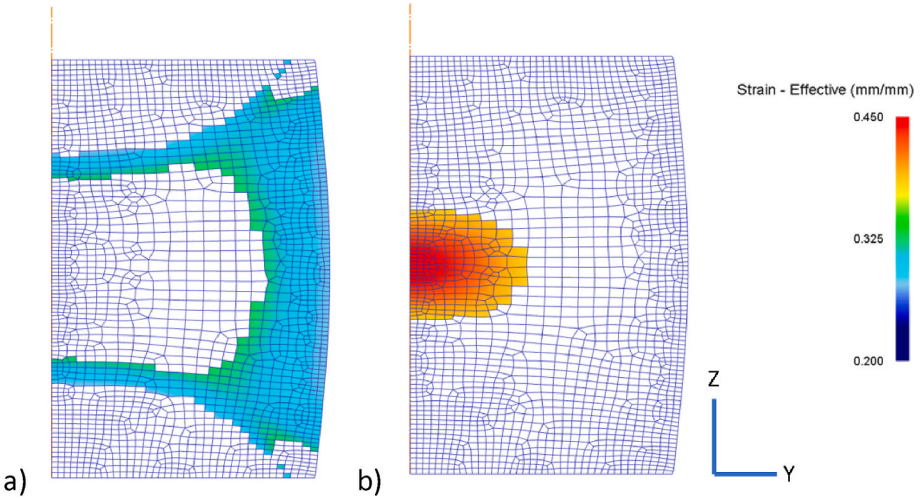

Fig. 3. Isolated region of a) 0.27–0.33 strain and b) 0.38–0.44 strain taken from the central Y-Z plane of UCT1.

sample core.

The simulation predicts a barrelling coefficient of 1.05 using a friction coefficient of 0.15 and uniform temperature, which is in agreement with modelling carried out by Bennet et al. [19]. However it has been reported in the literature [35] that for a high temperature testing (up to 1200 °C) thermal profiles can cause barrelling coefficients to be in excess of 1.15 and as such a much greater strain distribution is possible within samples. It should be noted that thermal gradient is more of a concern in direct joule heated samples such as in a Gleeble rather than furnace testing.

The UCT2 sample results follow a similar trend to those for the UCT1 sample, Fig. 4. The central region shows a slightly higher strain than in UCT1 of around 0.42 (Fig. 4), this is due to the samples aspect ratio being closer to 1, which results in the shear bands, formed in the corners due to friction, increasing their interaction with each other at a more focused point in the sample centre.

The UCT2 sample geometry shows a similar region of strain within ±0.03 (10%) of the macroscopically applied strain (39% volume of the sample) to the UCT1 sample. When sectioning the sample in the Y-Z plane then this would give 47 mm^2 of consistent strain for microstructural analysis (Fig. 5), which would allow quantification of around 600 grains of 250 μm diameter. The central region experiences a strain that is ~ 40% higher than the macroscopic strain and the region of uniform strain is only 11% of the cross section, which would allow 160 grains of 250 μm diameter to be measured, suggesting this geometry is no better for microstructural analysis than UCT1.

4.2. Plane strain compression

PSCT in systems such as a Gleeble or Servotest has conventionally used a geometry similar to that highlighted in Table 1. Although this geometry does not abide by the b/w = 5 ratio (sample width:anvil width) suggested by Watts and Ford [36] for true plane strain condition, the true stress and true strain can be calculate by the following equations:

$$\varepsilon = f \ln\left(\frac{h_o}{h}\right) \tag{2}$$

$$\sigma = \frac{\sigma_f}{f} \tag{3}$$

Where ε is the true strain, σ is the true stress, h_o and h are the initial and instantaneous sample height, σ_f is the flow stress, w is the sample width and f is the spread coefficient defined by:

$$f = \frac{1.155(b - w) + w}{b} \tag{4}$$

Fig. 6a shows the modelled strain distribution for the PSCT sample. It can be seen that there is significant strain variation through thickness. The shear bands formed from the corner of the anvils meet at the sample core to give a high local strain resulting in a bimodal strain distribution in the Y-Z plane (Fig. 6b), where the dead zone at the top and the uniform strain in the core are connected by a steep strain gradient. In the x axis, however, a region of around + -2.5 mm from the central axis shows a strain distribution that is much more consistent than that of uniaxial

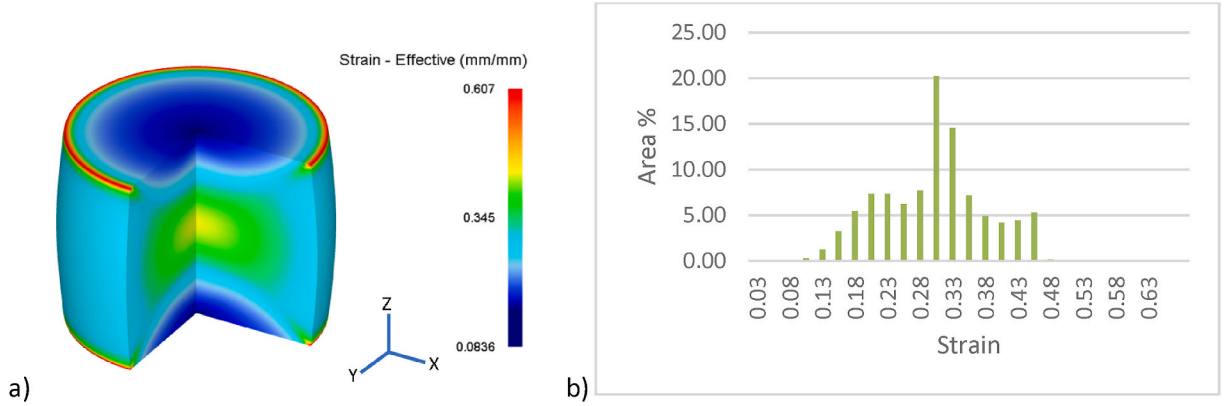

Fig. 4. Strain distribution in Uniaxial 2 at a macroscopic strain of 0.3 and b) histogram showing the sample area fraction experiencing the different strain levels.

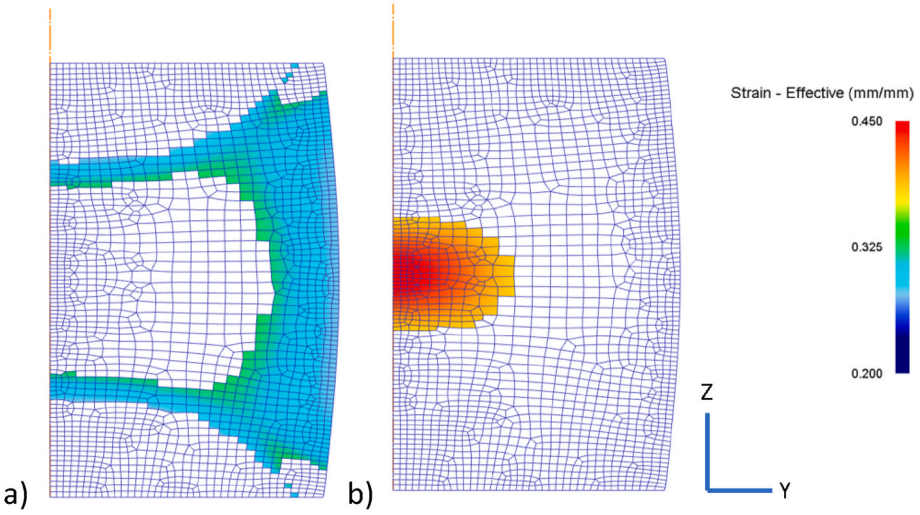

Fig. 5. Isolated region of a) 0.27–0.33 strain and b) 0.39–0.45 strain taken from the central Y-Z plane of UCT2.

compression UCT1 and UCT2 samples.

Fig. 7a shows the region of ±10% of the macroscopic 0.3 strain for the PSCT sample. There is a very small band where the strain is 0.27–0.33 which would not be appropriate for microstructural analysis as it would be difficult to section accurately to this location – for example to section in the X–Y plane to achieve a large microstructural region of uniform strain, since the 0.27–0.33 strain zone is < 1 mm thick in the Z-axis. Fig. 7b shows the region of largest consistent strain in the sample (0.44–0.5 for this sample), showing a band across the entire width of the sample. This region provides 31 mm^2 for analysis, moreover this region extends approximately ±2.5 mm thick in the x axis, which would allow 2–3 slices to be readily taken by sectioning for microstructural analysis to give analysis of >750 grains.

4.3. Modified plane strain compression

It was observed from the standard PSCT sample that shear strain generated from the corners of the anvils affect the core strain level in the central cross-section giving a higher local strain then macroscopically applied strain, with the severity of the shear strain being affected by the anvil geometry. Simulations were carried out increasing the anvil width, within the range possible within the Gleeble HDSV40 load capacity, until it was observed that the shear zones from the four anvil corners do not extend into the centre of the sample, giving more uniform strain in the core of the sample close to the macroscopically applied strain. The limitation to increasing the anvil width is the load capacity of the machine as well as the length of uniform hot zone that can be generated. For a Gleeble HDS-40 a hot zone of around 30 mm (length giving ± 5 °C from the core temperature) can be achieved and therefore 20 mm anvils are most appropriate to ensure all deformation is constrained in the hot zone, however for plane strain testing using a furnace to heat samples larger anvils could potentially be used to generate the region of uniform strain provided this is within any space constraints and load capacity of the machine (which will depend on the material and the test temperature).

Fig. 8a shows the strain distribution in this new sample geometry, of 50 × 20 × 10 mm (LxWxH) and an anvil width of 20 mm. The strain through thickness at the central cross-section is more uniform than in Fig. 6 With an average of 0.3 strain, Fig. 8b shows the tight normal distribution of the area percentage against strain obtained from this geometry sample. In addition, this sample shows in a region of ±5 mm in the x axis (double that of the standard PSCT) that shows a consistent strain pattern and minimal interaction from the shear bands formed from the anvil corners, which allows multiple sections to be taken for microstructural examination, and also sectioning accuracy becomes less critical.

Fig. 9 shows the distribution of uniform strain in the modified PSCT sample. A significant increase in strain uniformity can be seen, in particular the region of 0.3 strain ±10% is much increased (around 122 mm^2). This can be refined to a tighter tolerance of ±5% of the target strain (Fig. 9b) where 78 mm^2 falls within this range, allowing over 1500 grains for analysis from a single slice through the sample. The distribution of the consistent strain region is much more suitable for metallographic assessment. There is however, a region at the core that has a strain of 0.36. It is therefore suggested that a region of 6 × 6mm taken at the ¼ width of the sample (shown by the green box in Fig. 9b) gives excellent homogeneity and consistency with the macroscopic imposed strain allowing the best control and accuracy for recrystallisation studies.

Table 2 summarises the strain distributions obtained by modelling from the four sample geometries, where the central region of consistent strain is much higher than the applied strain and is restricted to a relatively small region for the standard samples (UCT1, UCT2 and PSCT). Although using the region of higher strain gives a better region for metallographic assessment, the higher strain than that which was macroscopically applied makes test matrix particularly as this will have a knock-on impact on the strain rate and also any inter-pass time calculations during multi-pass simulations.

The proposed modified plane strain geometry provides not only a larger area for analysis, but also increases the accuracy of the strain (both in terms of distribution but also in its agreement to the macroscopically applied strain).

4.4. Experimental verification

Samples of 316 stainless steel were tested in all 4 geometries shown in Table 2. The true flow stress curves can be seen in Fig. 10 (which were calculated using Equations (2)–(4) for plane strain and classical true stress/strain equations for uniaxial tests). The flow curves and the 5% proof stress for all geometries are very similar with the exception of PSCT which shows a much higher proof stress. This is consistent with Fig. 6b which showed the highest local strain, this in turn would result in the sample locally reaching the yield stress much earlier in the deformation compared to the other samples.

Fig. 11 shows the hardness maps for the four geometries, all on the Y-Z plane at the central location (X = 0) equivalent to the strain maps shown in Figs. 3, 5, 7 and 9, which have been summarised as a histogram for the relative frequency of hardness values in Fig. 12. As with the flow

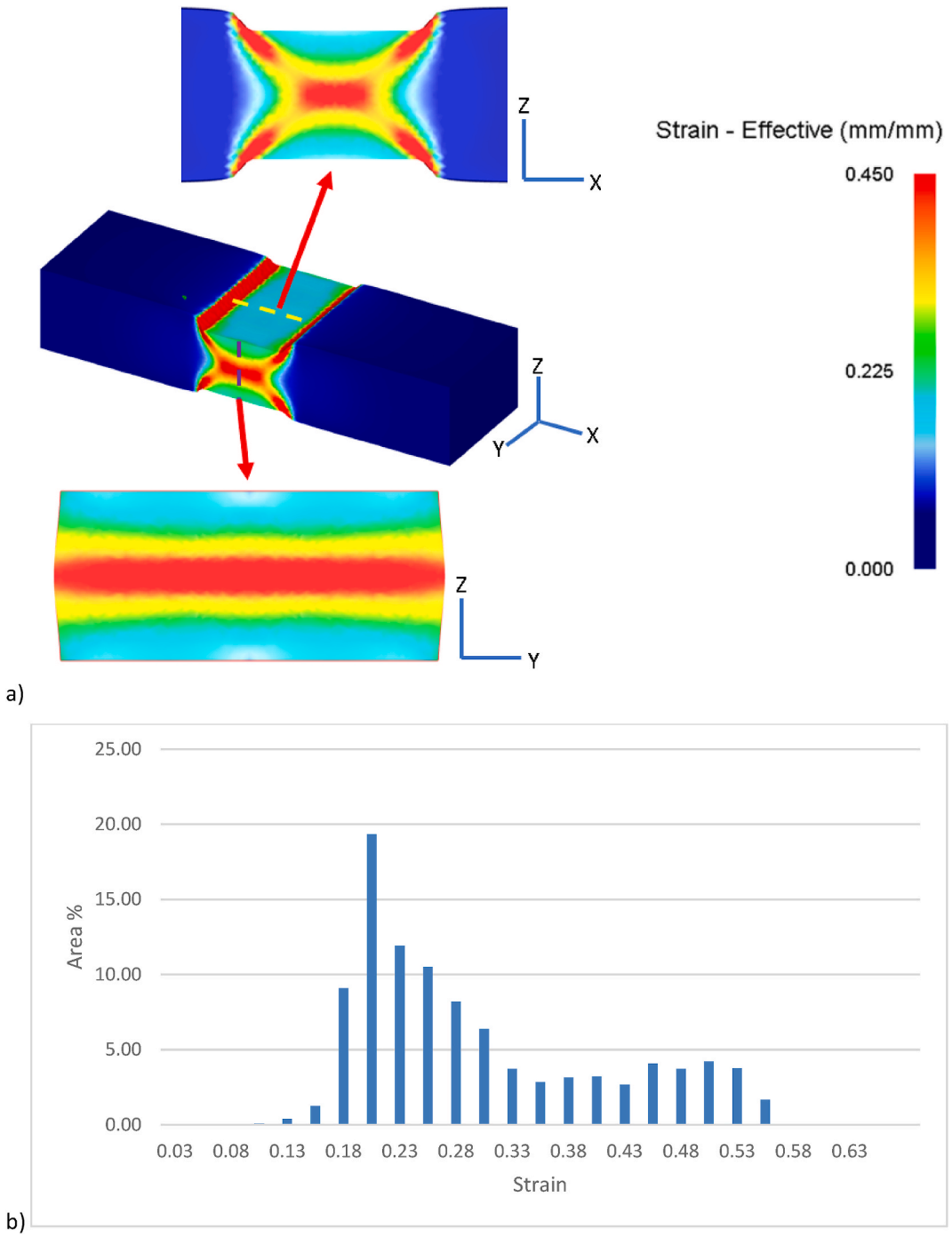

Fig. 6. a) Strain distribution in the PSCT sample geometry highlighting a slices from the Y-Z and X-Z planes from the centre of the deformation region and b) a histogram of area percentage at given strain values in the sliced region.

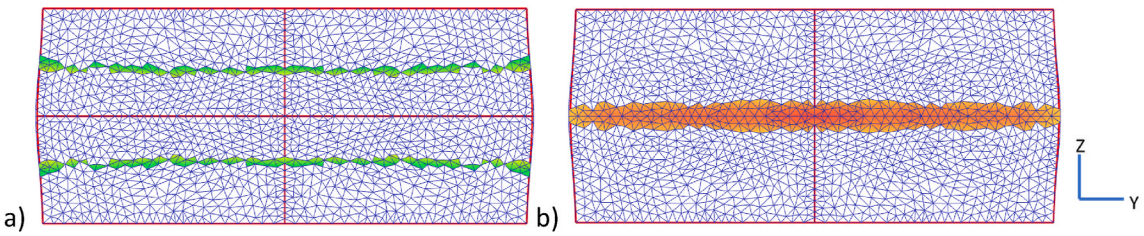

Fig. 7. Isolated region of a) 0.27–0.33 strain and b) 0.44–0.5 strain taken the Y-Z plane from the centre of the deformed region of the PSCT sample.

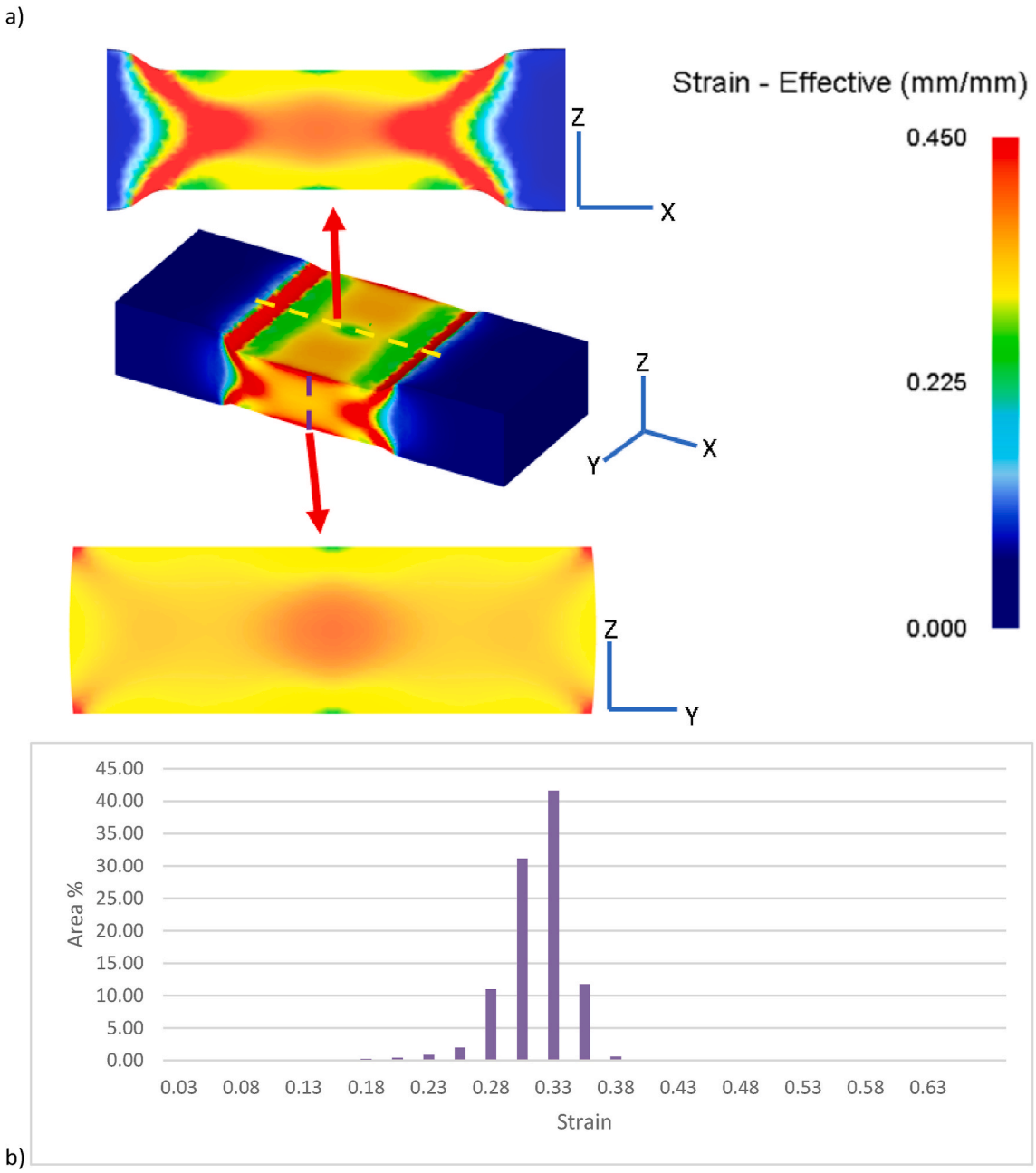

Fig. 8. a) Strain distribution in the Modofied PSCT sample geometry highlighting slices from the Y-Z and X-Z planes from the centre of the deformation region and b) a histogram of area percentage for different strain of the Y-Z plane slice region.

curves, PSCT shows a significantly larger range in hardness values compared to the other geometries. Both the modified PSCT and UCT1 show a mode hardness of 265 HV compared to the higher 285 HV seen in UCT2.

The hardness values have been translated to an imposed strain value using the factor of 3.03 to convert the hardness to a stress and then relating the stress to an imposed strain from Fig. 1. Fig. 13 shows composite images made up from the predicted and measured regions of 0.3 ± 10% strain for all four sample geometries deformed to a macroscopically applied 0.3 strain. Good agreement can be seen for both the plane strain samples. UCT2 shows the high strain region at the core (Fig. 11), but the predicted dead zone at the top and bottom of the sample seems to be very small/not picked up by the hardness map, suggesting a lower friction coefficient occurred than used in the modelling. UCT1 however does not show good correlation between predicted and measured profiles. The uniaxial samples are very sensitive to small errors in sectioning and the amount of material that is removed during the preparation (grinding and polishing) stage. It can also be seen that the sample shows asymmetry with the bottom of the sample showing a larger dead zone than the top, suggesting a difference in friction coefficient (although the diameter at either end of the sample varied by < 0.2 mm), or a non planar section taken from the sample. This highlights further the sensitivity of the complex strain profiles seen in the UCT tests. Fig. 14 shows the inherent variability of the UCT testing approach, where direct repeat tests under identical conditions show variation in the strain spatial distribution (repeat tests showed the same flow stress curves in each case, and therefore the variability is local rather than related to the global test setup). Although large portions of all these samples fall within the ±10% of 0.3 strain, the location of these regions is not stable, making consistent microstructural assessment difficult. These tests have been carried out using brand new anvils and therefore the performance of these tests would be expected to decrease

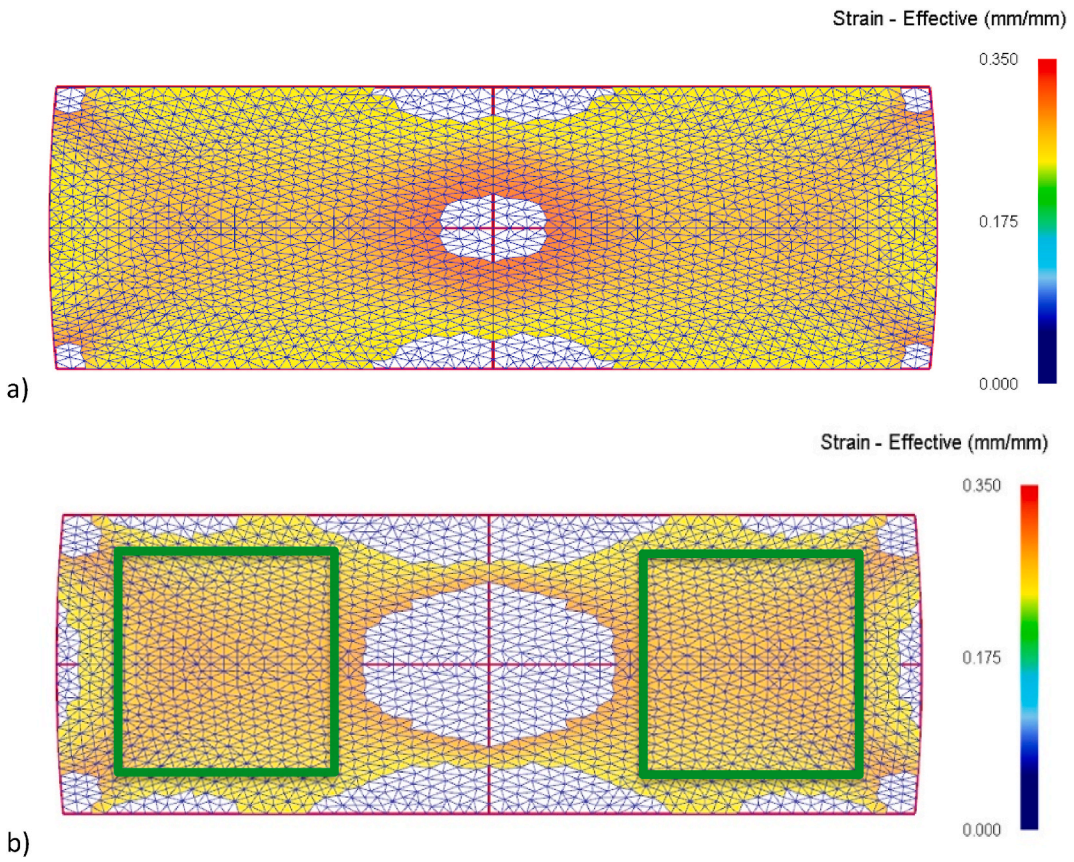

Fig. 9. Isolated region of a) 0.27–0.33 strain and b) 0.285–0.315 strain taken the Y-Z plane from the centre of the deformed region of the modified PSCT sample. A region appropriate for metallographic assessment has been highlighted in the green boxes.

Table 2
Summary of the strain distributions through the 4 geometries modelled.

Sample	Average Strain	Size of region of ±10% applied strain (mm^2)	Strain at section appropriate for metallographic examination	Size of core region (mm^2)
UCT1	0.278	52	0.38–0.44	13
UCT2	0.284	47	0.39–0.45	13.5
PSCT	0.295	25	0.44–0.5	32
Modified PSCT	0.3	122	0.285–0.315	36 × 2

with more practical (i.e. partially worn) anvil conditions.

4.5. Sectioning sensitivity

Further variability between tests can be sourced to sectioning accuracy. A typical diamond blade cutting wheel has a thickness of around 0.5 mm, where sectioning cutting locations, non-planar cuts and the level of grinding before final polish, all adding to inaccuracies in the precise location of the comparison between the experimental data sets.

The variability/consistency of the different compression methods can be seen in Fig. 15 where the strain distribution in the Y-Z plane has been plotted at various offsets to the central plane. It can be seen that the strain distribution in the modified PSCT even at 5 mm away from the central axis remains almost identical, allowing for multiple slices to be taken but also allows for a larger degree of error when sectioning the sample. The UCT sample however, shows varying strain patterns for the different slices, with 5 mm away from the central axis showing almost no dead zone but a higher proportion of 0.3 strain. Whilst the mode at this section shows a more preferential distribution, the variability with sectioning plane means that poor repeatability/consistency would be expected. The reduction in the proportion of the dead zone with increasing distance away from the central slice helps understand some of the variability and lack on dead zone seen Fig. 15. Any sectioning inaccuracy leads to a surface off the midplane being analysed, with the section out of the Y-Z plane explaining the asymmetry at the top and bottom of the UCT samples. Whilst cutting and grinding consistency can be improved, it is important to show here the variability that can arise even when producing a small number of samples. For this, the PSCT sample shows much more repeatability and less sensitivity to small variations in preparation.

In addition to the PSCT showing a much larger strain variation, the excellent correlation between the predicted and measured strain makes this test much more reliable. Moving to a 20 mm anvil size, as with the modified PSCT sample, gives a predictable large area of uniform strain and offers the best setup for microstructural analysis post testing.

4.6. The ideal section

Considering all of the above, then the ideal section will have the following traits:

- Uniform strain.
- Strain that corresponds to the macroscopically applied strain.
- Area of uniform strain is distributed such to be appropriate for metallographic assessment.
- Has good tolerance to inaccuracies during sectioning and preparation.

Then the ideal section can be seen in Fig. 16 which is taken in the x-z plane at the ¼ and ¾ position in the y axis. This has the added benefit of

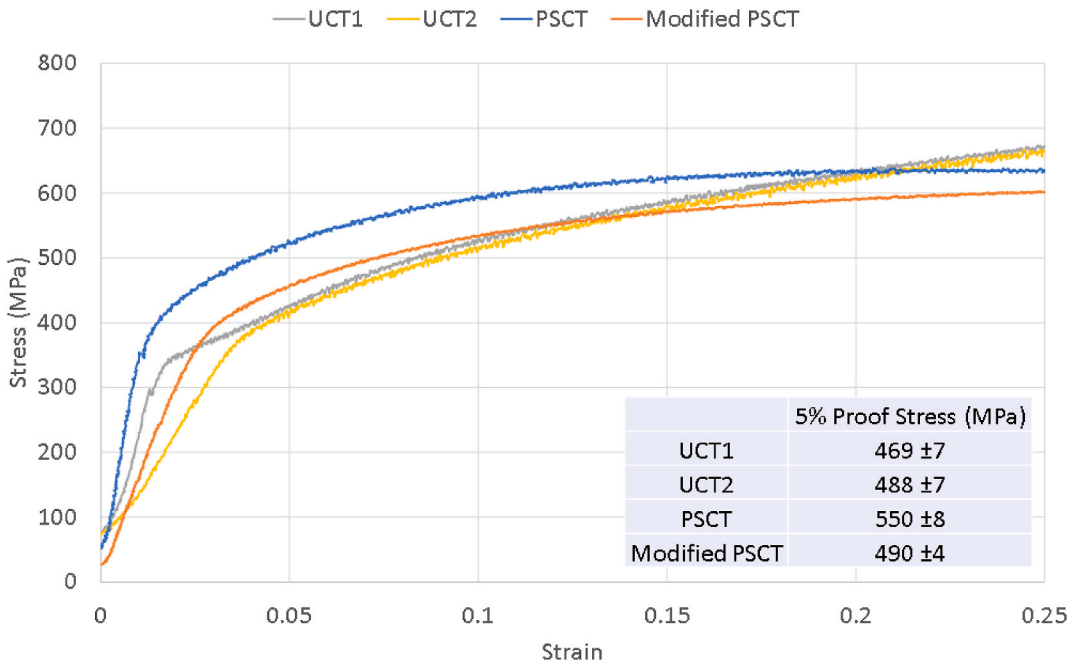

Fig. 10. Stress/Strain curves for the four different compression geometries.

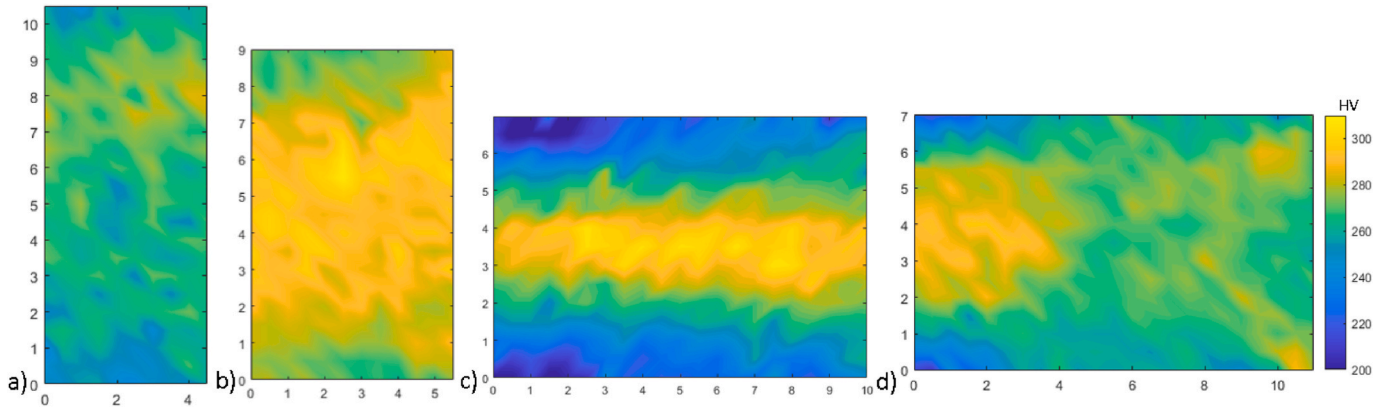

Fig. 11. Hardness maps for a) UCT1, b) UCT2, c) PSCT and d) modified PSCT on the Y-Z plane at X = 0 (mid position).

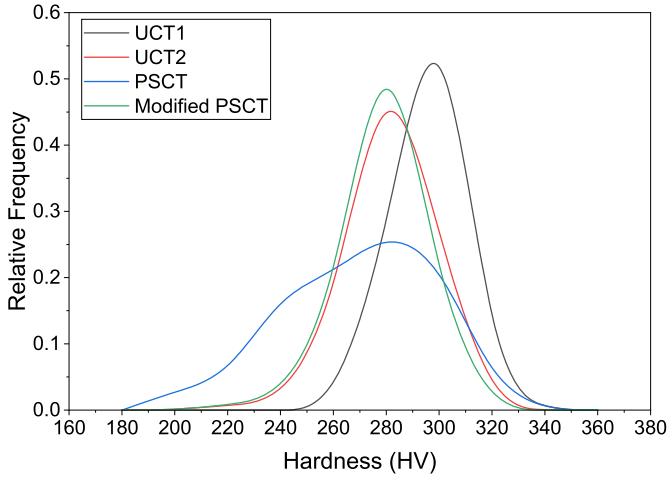

Fig. 12. Hardness histograms for the four compression geometries taken from the Y-Z plane at X = 0 (mid position).

being in the deformation plane and as such is equivalent to looking at the rolling axis of strip products formed during rolling. This is the suggested best section that can be achieve for microstructural analysis of recrystallisation within the limits of lab based thermo-mechanical testing equipment. For softer alloys such as copper and aluminium, then wider anvils will give even greater strain uniformity for metallographic analysis, although this would provide minimal improvement to the accuracy of the flow stress curves.

5. Conclusions

Lab based recrystallisation studies are important for determining optimum industrial processing conditions (strain, temperature, strain rate) to achieve desired microstructural refinement. Several methods have been developed to characterise recrystallisation including uniaxial compression testing (UCT) and plane strain compression testing (PSCT). Flow stress analysis (double hit tests or stress relaxation) are used to determine recrystallisation kinetics, however microstructural analysis is required to determine recrystallisation grain sizes/grain size distributions and can also be used to assess recrystallisation kinetics. A high degree of strain homogeneity is required in the sample to give sufficient

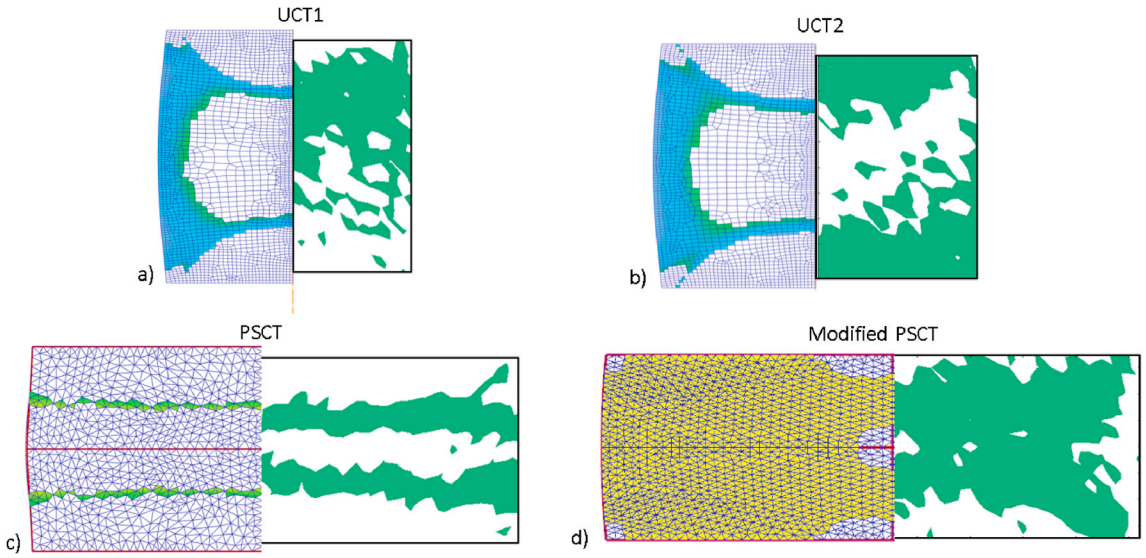

Fig. 13. Composite images showing the predicted region (left) and measured through hardness mapping (right), highlighting the region that falls within ±10% of 0.3 strain for a) UCT1, b) UCT2, c) PSCT and d) modified PSCT.

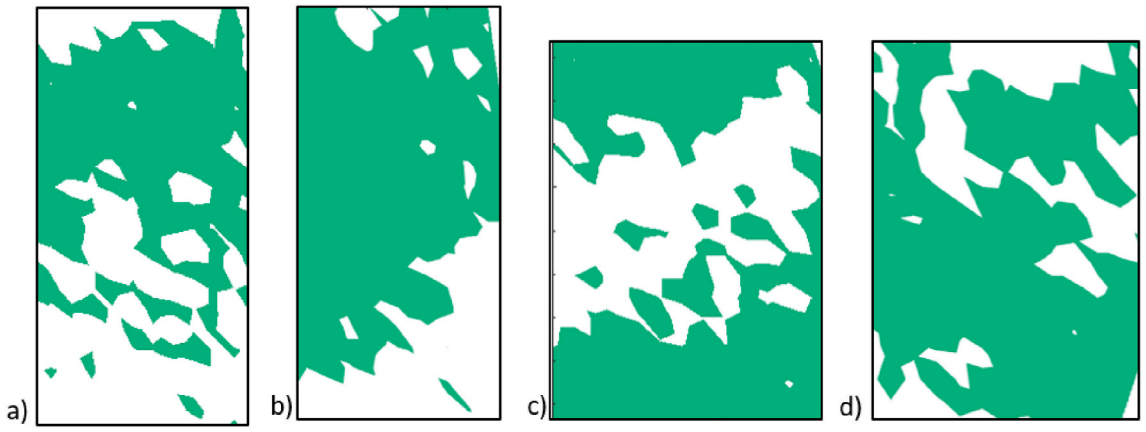

Fig. 14. Hardness mapping indicating region of 0.3 strain ±10% for a) UCT1, b) UCT1 repeat, c) UCT2 and d) UCT2 repeat.

area for microstructural analysis. This paper considers the strain distribution in the most common compression test geometries used for recrystallisation studies and compares the strain distribution uniformity and area of uniform strain for metallographic assessment. Modelling and experimental validation has been used and a modified PSCT sample geometry is proposed. The main conclusions are:

Both commonly used UCT sample geometries showed with an applied global strain of 0.3 showed a core strain of 0.4 and 0.42. In addition to this, although around 50 mm^2 of fell with ±10% of the applied strain, the distribution of this strain makes metallographic assessment difficult as even small offsets from the ideal cross section position reduces this uniform strain area.

A standard plane strain geometry using 10 mm anvils showed a strong through thickness variation in strain with an average core strain of 0.5. With only a small area achieving the desired strain.

A modified plane strain sample has been suggested which generates much greater uniformity of strain providing an area of 122 mm^2 with ±10% of the applied strain on a cross section slice. Over twice the amount of any other geometry, but also more favourably spatially distributed.

Experimental verification was carried out using stainless steel 316 in a Gleeble HDS-V40 for the different sample geometries followed by microhardness mapping. Good agreement was seen between the modelled and experimental strain values for the plane strain sample geometries, however uniaxial compression testing showed large amounts of asymmetry and variability between repeat tests (consistent with the proposed susceptibility of the sample to sectioning errors).

Appreciation for accuracy needed during section was also taken into consideration, with the plane strain samples showing a much greater tolerance to inaccuracies of cutting and grinding of samples to assess the central plane.

Therefore, it is suggested that for metallographic assessment of recrystallisation, such as recrystallised grain size distributions, a plane strain sample geometry sample tested with >20 mm width anvils provides excellent strain uniformity in the samples and a large area suitable for microstructural characterisation.

Author statement

Carl Slater: Conceptualization, Methodology, Formal analysis, Investigation, Writing – original draft. Nusrat Tamanna: Software, Visualization. Claire Davis: Writing – review & editing, Supervision.

Declaration of competing interest

The authors declare that they have no known competing financial

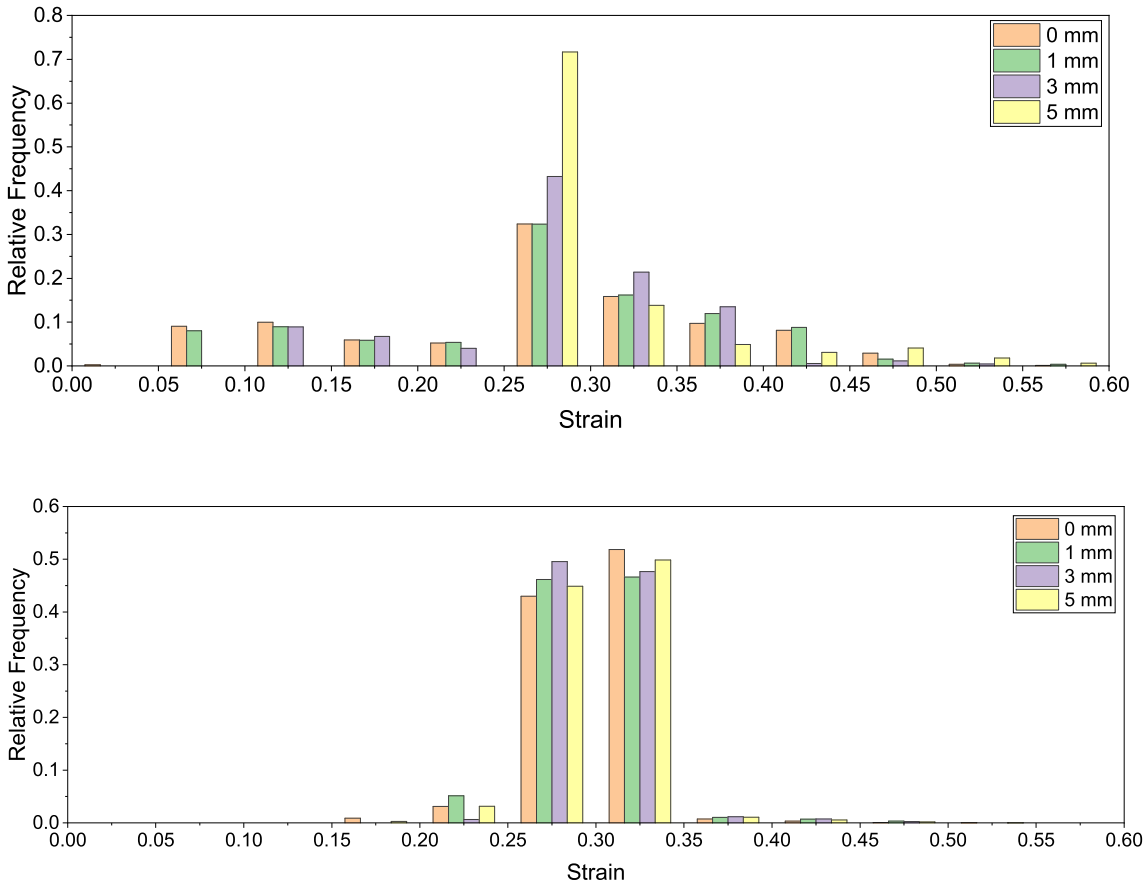

Fig. 15. Strain distributions in the Y-Z plane taken at various X offsets from the central plane for a) UCT1 and b) modified PSCT.

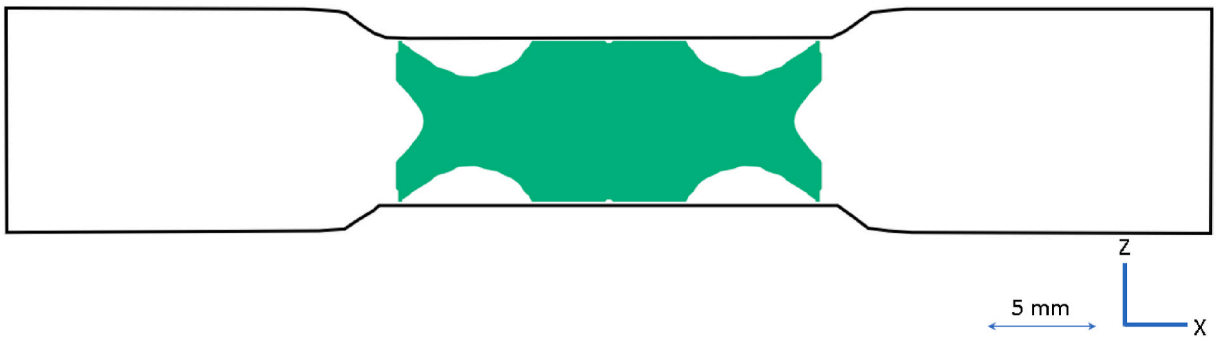

Fig. 16. Schematic showing the ideal section showing the region of strain between 0.27 and 0.33 taken from the x-z plane at the quarter/three quarter position in the y axis.

interests or personal relationships that could have appeared to influence the work reported in this paper.

Acknowledgements

The authors would like to thank the High Value Manufacturing Catapult at WMG for their ongoing support for the research.

References

[1] B. López, J.M. Rodriguez-Ibabe, Recrystallisation and Grain Growth in Hot Working of Steels, Woodhead Publishing Limited, 2012, https://doi.org/10.1533/9780857096340.1.67.

[2] E.I. Galindo-Nava, C.M.F. Rae, Microstructure evolution during dynamic recrystallisation in polycrystalline nickel superalloys, Mater. Sci. Eng. 636 (2015) 434–445, https://doi.org/10.1016/j.msea.2015.03.121.

[3] J. Schamp, B. Verlinden, J. Van Humbeeck, Recrystallisation at ambient temperature of heavily deformed ETP copper wire, Scripta Mater. 34 (1996) 1667–1672, https://doi.org/10.1016/1359-6462(96)00034-6.

[4] R. Kumar, A. Gupta, A. Kumar, R.N. Chouhan, R.K. Khatirkar, Microstructure and texture development during deformation and recrystallisation in strip cast AA8011 aluminum alloy, J. Alloys Compd. 742 (2018) 369–382, https://doi.org/10.1016/j.jallcom.2018.01.280.

[5] D.Z. Yang, E.L. Brown, D.K. Matlock, G. Krauss, Ferrite recrystallization and austenite formation in cold-rolled intercritically annealed steel, Metall. Trans. A. 16 (1985) 1385–1392, https://doi.org/10.1007/BF02658671.

[6] B.S. Murty, S.A. Kori, M. Chakraborty, Grain refinement of aluminium and its alloys by heterogeneous nucleation and alloying, Int. Mater. Rev. 47 (2002) 3–29, https://doi.org/10.1179/095066001225001049.

[7] G. Yao, C. Cao, S. Pan, J. Yuan, I. De Rosa, X. Li, Thermally stable ultrafine grained copper induced by CrB/CrB2 microparticles with surface nanofeatures via regular casting, J. Mater. Sci. Technol. 58 (2020) 55–62, https://doi.org/10.1016/J.JMST.2020.03.052.

[8] I. Tamura, H. Sekine, T. Tanaka, C. Ouchi, Introduction. Thermomechanical Process. High-Strength Low-Alloy Steels, Elsevier, 1988, pp. 1–16, https://doi.org/10.1016/b978-0-408-11034-1.50004-0.
[9] J. Zhao, Z. Jiang, Thermomechanical processing of advanced high strength steels, Prog. Mater. Sci. 94 (2018) 174–242, https://doi.org/10.1016/j.pmatsci.2018.01.006.
[10] J.H. Beynon, C.M. Sellars, Modelling rolling microstructure and its effects during multipass hot by collaborative work the sheffield leicester integrated model for microstructural evolution in rolling, ISIJ Int. 32 (1992) 359–367.
[11] M. Ji, V. Janik, M. Strangwood, C. Davis, Effect of grain size distribution on recrystallisation kinetics in a Fe-30Ni model alloy, in: E.A. Holm, S. Farjami, P. Manohar, G.S. Rohrer, A.D. Rollett, D. Srolovitz, H. Weiland (Eds.), Proc. 6th Int. Conf. Recryst. Grain Growth (ReX&GG 2016), Springer International Publishing, Cham, 2016, pp. 153–158.
[12] B. Pereda, J.M. Rodriguez-Ibabe, B. López, Improved model of kinetics of strain induced precipitation and microstructure evolution of Nb microalloyed steels during multipass rolling, ISIJ Int. 48 (2008) 1457–1466, https://doi.org/10.2355/isijinternational.48.1457.
[13] S. Bao, G. Zhao, C. Yu, Q. Chang, C. Ye, X. Mao, Recrystallization behavior of a Nb-microalloyed steel during hot compression, Appl. Math. Model. 35 (2011) 3268–3275, https://doi.org/10.1016/j.apm.2011.01.024.
[14] C. Iparraguirre, A.I. Fernández-Calvo, B. López, Effect of initial austenite microstructure on the softening – precipitation interaction in a low Nb microalloyed steel, Mater. Sci. Forum 550 (2007) 429–434. https://doi.org/10.4028/www.scientific.net/msf.550.429.
[15] Gleeble, https://www.gleeble.com/ (accessed 18.08.2021).
[16] Servotest, https://www.servotestsystems.com/ (accessed 18.08.2021).
[17] X.G. Fan, Y.D. Dong, H. Yang, P.F. Gao, M. Zhan, Friction assessment in uniaxial compression test: a new evaluation method based on local bulge profile, J. Mater. Process. Technol. 243 (2017) 282–290, https://doi.org/10.1016/j.jmatprotec.2016.12.023.
[18] A. Chamanfar, H.S. Valberg, B. Templin, J.E. Plumeri, W.Z. Misiolek, Development and validation of a finite-element model for isothermal forging of a nickel-base superalloy, Materialia 6 (2019), https://doi.org/10.1016/j.mtla.2019.100319.
[19] C.J. Bennett, S.B. Leen, E.J. Williams, P.H. Shipway, T.H. Hyde, A critical analysis of plastic flow behaviour in axisymmetric isothermal and Gleeble compression testing, Comput. Mater. Sci. 50 (2010) 125–137, https://doi.org/10.1016/j.commatsci.2010.07.016.
[20] M. Gómez, S.F. Medina, P. Valles, Determination of driving and pinning forces for static recrystallization during hot rolling of a niobium microalloyed steel, ISIJ Int. 45 (2005) 1711–1720, https://doi.org/10.2355/isijinternational.45.1711.
[21] S.F. Medina, P. Fabregue, Activation energy in the static recrystallization of austenite, J. Mater. Sci. 26 (1991) 5427–5432, https://doi.org/10.1007/bf00553641.
[22] David R. Forrest, M.F. Sinfield, Numerical Simulation of Gleeble Torsion Testing of HSLA-65 Steel, 2008. West Bethesda.
[23] DSI, Application Notes - APN002, 2003. https://www.gleeble.com/resources/application-notes.html.
[24] H. Xiao, X.G. Fan, M. Zhan, B.C. Liu, Z.Q. Zhang, Flow stress correction for hot compression of titanium alloys considering temperature gradient induced heterogeneous deformation, J. Mater. Process. Technol. 288 (2021) 116868, https://doi.org/10.1016/j.jmatprotec.2020.116868.
[25] M.K.M. Kaonda, Prediction of the Recrystallised Grain Size Distribution after Deformation for the Nb Free and Nb Model Steel, 2017. http://etheses.bham.ac.uk/7680/1/Kaonda17PhD.pdf.
[26] C. Slater, A. Mandal, C. Davis, The influence of segregation of Mn on the recrystallization behavior of C-Mn steels, Metall. Mater. Trans. B Process Metall. Mater. Process. Sci. 50 (2019), https://doi.org/10.1007/s11663-019-01603-2.
[27] P. Kalinowski, C.L. Davis, M. Strangwood, Recrystallisation and Grain Size Development During Forging in Power Generation Steels, (n.d.).
[28] A. Kundu, C.L. Davis, M. Strangwood, Modeling of grain size distributions during single hit deformation of a Nb-containing Steel, Metall. Mater. Trans. 41 (2010) 994–1002.
[29] C.N. Athreya, S. Suwas, V.S. Sarma, Role of stress state on dynamic recrystallization behaviour of Ni during hot deformation: analysis of uniaxial compression and plane strain compression, Mater. Sci. Eng. 763 (2019) 138153, https://doi.org/10.1016/j.msea.2019.138153.
[30] A. Chamanfar, M. Jahazi, J. Gholipour, P. Wanjara, S. Yue, Evolution of Flow Stress and Microstructure during Isothermal Compression of Waspaloy, 2014, https://doi.org/10.1016/j.msea.2014.07.093.
[31] C. Herrera, A.F. Padilha, R.L. Plaut, Microstructure evolution during annealing treatment of austenitic stainless steels. Recryst. Grain Growth IV, Trans Tech Publications Ltd, 2012, p. 913. https://doi.org/10.4028/www.scientific.net/MSF.715-716.913.
[32] J.T. Busby, M.C. Hash, G.S. Was, The relationship between hardness and yield stress in irradiated austenitic and ferritic steels, J. Nucl. Mater. 336 (2005) 267–278, https://doi.org/10.1016/j.jnucmat.2004.09.024.
[33] M. Kosta, M. Kaonda, C. Slater, M. Strangwood, C. Davis, Modelling the Recrystallised Grain Size Distribution After Deformation, (n.d.).
[34] a. Kundu, Grain Structure Development During Casting, Reheating and Deformation of, Development., 2011, p. 354.
[35] X. Wang, H. Li, K. Chandrashekhara, S.A. Rummel, S. Lekakh, D.C. Van Aken, R. J. O'Malley, Inverse finite element modeling of the barreling effect on experimental stress-strain curve for high temperature steel compression test, J. Mater. Process. Technol. 243 (2017) 465–473, https://doi.org/10.1016/j.jmatprotec.2017.01.012.
[36] A.B. Watts, H. Ford, On the basic yield stress curve for a metal, Proc. Inst. Mech. Eng. 169 (1955) 1141–1156, https://doi.org/10.1243/PIME_PROC_1955_169_111_02.